

Optical and structural investigations on iron-containing phosphate glasses

M. Elisa · R. Iordanescu · B. A. Sava · G. Aldica ·
V. Kuncser · C. Valsangiacom · G. Schintieie · F. Nastase ·
C. Nastase · V. Bercu · A. Volceanov · S. Peretz

Received: 4 May 2010 / Accepted: 29 September 2010 / Published online: 14 October 2010
© Springer Science+Business Media, LLC 2010

Abstract The article reports the preparation and complex characterization of iron-containing phosphate glasses considered to be ecological materials, as they contain non-toxic compounds related to environment. The oxide system $\text{Li}_2\text{O}-\text{MgO}-(\text{CaO})-\text{Al}_2\text{O}_3-\text{P}_2\text{O}_5-(\text{FeO}/\text{Fe}_2\text{O}_3)$ was investigated in respect to its structural changes caused by MgO replacement with CaO and by the iron addition. UV-vis-NIR (ultraviolet-visible-near infrared) spectroscopy as well as thermo-gravimetric (TG) measurements, differential thermo-analysis (DTA), X-ray diffraction (XRD)

analysis, electronic paramagnetic resonance (EPR), and Mossbauer (nuclear gamma resonance) spectroscopy have been used to investigate redox states and coordination symmetry of iron, together with vitreous network changes during the heat treatment up to 1000 °C. UV-vis-NIR transmission spectroscopy revealed no structural modifications when MgO was substituted by CaO, but noteworthy absorption bands attributed to $\text{Fe}^{2+}/\text{Fe}^{3+}$ species. TG analysis made in the 20–1000 °C range shows low weight loss accompanied by several thermal effects, as evidenced by DTA. XRD patterns for the glass samples heat treated at about 700 °C revealed the presence of different phosphate crystalline phases containing Mg, Al, and Fe ions. EPR spectroscopy revealed the presence of paramagnetic Fe^{3+} ions and the change of the first coordination symmetry, when the samples are heated below the vitreous transition temperature. Mossbauer spectroscopy has evidenced two paramagnetic species, Fe^{2+} and Fe^{3+} , both in octahedral coordination symmetry and a clustering process supported by only Fe^{3+} ions.

M. Elisa (✉) · R. Iordanescu
Optospintrronics Laboratory, National Institute of Research and Development for Optoelectronics—INOE 2000, 409 Atomistilor Str, P.O. MG-5, 77125 Magurele, Romania
e-mail: astatin18@yahoo.com

B. A. Sava
Optical Glass Laboratory, National Institute of Glass, Bucharest, Romania

G. Aldica · V. Kuncser · C. Valsangiacom · G. Schintieie
Magnetism and Superconductivity Department, National Institute of Materials Physics, Magurele, Romania

F. Nastase · C. Nastase
Polymer Science Group, Faculty of Physics, University of Bucharest, Magurele, Romania

V. Bercu
Department of Atomic and Nuclear Physics, Faculty of Physics, University of Bucharest, Magurele, Romania

A. Volceanov
Faculty of Applied Chemistry and Materials Science, Politehnica University of Bucharest, P.O.Box 12-134, Bucharest, Romania

S. Peretz
Department of Colloids, Institute of Physical Chemistry I.Murgulescu, Bucharest, Romania

Introduction

It is well known that different oxidation states of the transition metal ions as well as their distribution in the glass network strongly influence the electrical, optical, and magnetical properties of these materials [1–3].

Recently, phosphate glasses gained a real scientific interest due to their low melting temperature as well as their ability to embed high amounts of alkali oxides and transition metal oxides as well as sulfides and molybdenites. Phosphate glasses are also able to retain the radioactive wastes enriched in sodium and sodium aluminates, wastes that contain products of the uranium fission (radio

nuclei of cesium, strontium, rare-earth, etc.), corrosion products from nuclear reactors (radio nuclei of iron, cobalt, nickel, and manganese), compounds of the nuclear fuel (uranium and plutonium), and impurities of the nuclear process (sulfides, chlorides) [4]. Iron oxides (FeO and Fe_2O_3) used as doping compounds, also influence the structure and properties of the phosphate glasses [5]. Small amounts (2–5%) of Fe_2O_3 increase drastically (10^4 times) the chemical strength against water [6]. Thus, iron-doped phosphate glasses are very convenient to embed aqueous nuclear wastes [7].

Recently, non-polluting syntheses for glassware are taken into account, the toxic raw materials being replaced by non-harmful compounds. Thus, TiO_2 , ZrO_2 , ZnO and K_2O , MgO , SrO , La_2O_3 , Bi_2O_3 and Nb_2O_5 replaced PbO and BaO from the composition of the crystal glass. Compounds as MgO , Al_2O_3 , P_2O_5 , and B_2O_3 , replaced the corrosive fluorine from the composition of the opal glass [8].

This article reports a study (UV-vis-NIR spectroscopy, TG-DTA, XRD, EPR, and Mossbauer spectroscopy) on ecological phosphate glass containing iron ions. The results of the up-mentioned analyses will provide useful information on glass structure as well as the oxidation state and coordination symmetry of iron within the vitreous network. This work also investigates the influence of alkali-earth ions, Mg^{2+} , and Ca^{2+} over the oxidation states and coordination symmetry of iron ions in the glass network.

Experimental

The oxide composition of the starting glass batches is presented in Table 1.

The chemical reagents used for the glass preparation were: Li_2CO_3 , Al_2O_3 , MgCO_3 , CaCO_3 , H_3PO_4 , $\text{FeSO}_4 \cdot 7\text{H}_2\text{O}$, and all of analytical grade. The glass samples C1, C2, C3, and C4 were melted at 1200 °C for 2 h and subsequently, annealed according to the heat diagram resulted from the thermal expansion measurements [9]. The synthesis stages of the phosphate glasses were: (i) homogenization and evaporation of the reagents up to 100–120 °C, in quartz crucible; (ii) drying process at 180–200 °C; (iii) preliminary heat treatment

Table 1 Ecological phosphate glass batch compositions

Glass samples	Oxide composition (mol%)					
	Li_2O	MgO	CaO	Al_2O_3	Fe_2O_3	P_2O_5
C1	19.73	6.57	–	9.86	–	63.81
C2	19.73	–	6.57	9.86	–	63.81
C3	11.07	4.21	–	5.59	4.21	74.89
C4	11.07	–	4.21	5.59	4.21	74.89

at 200–

800 °C; (iv) glass melting and refining at 1200 °C; (v) casting, and (vi) annealing stage [10–13]. According to Table 1, the iron-doped samples C3 and C4 contain either MgO (sample 3) or CaO (sample 4). Also the first two samples are either with MgO (sample 1) or with CaO (sample 2), but without Fe.

The UV-vis-NIR spectroscopy was made by means of a Jasco V-570 spectrophotometer, in the range 190–2500 nm, in transmission geometry with 2 nm spectral resolution.

The TG-DTA analysis was performed by SETARAM Setsys Evolution 18, in TG-DSC Thermal Analyzer mode. Samples with a mass around 11 mg which was maintained constantly were measured in an open cylindrical alumina crucible. The experiments were conducted in flowing synthetic air (80% N_2 /20% O_2), at a flow rate of 16 mL/min. The temperature scan was between 300 and 1000 °C with a heating rate of 10 °C/min, within a precision in temperature better than 0.01 °C.

The XRD characterization was made by means of a Bruker D8 Advance X-Ray Solutions device, using a $\text{CuK}\alpha$ radiation.

The EPR spectra were recorded in the X-band (9.5 GHz) with a CMS 8400 Adani spectrometer provided with a H102 cylindrical resonator cavity and 100 kHz modulation field. The measurement error for the line position is ± 1.5 G for narrow lines and ± 5 G for broad lines. The magnetic field sweep has been calibrated by using CaO:Mn^{2+} standard sample.

Mossbauer spectra were acquired at room temperature, by using a classical set-up with triangular wave form and a ^{57}Co radioactive source in Rh matrix, with an initial activity of 50 mCi. The isomer shifts were reported relative to room temperature α -Fe with errors lower than 0.03 mm/s. Low temperature measurements were done by inserting the sample in a Janis close-cycle cryostat.

Results and discussion

The UV-vis-NIR transmission spectra for C1 and C2 samples, in the wavelength range from 300 to 2500 nm (Fig. 1), were quite similar and revealed a high transparency (about 90%) characteristic for phosphate glasses without absorbing impurities.

The iron-doped samples show a much lower transmission (Fig. 2). An absorption band specific to Fe^{3+} ions is observed at 457 nm and those specific to Fe^{2+} ions are noticed at 1084 and 2250 nm. No important modifications of the absorption bands due to MgO substitution by CaO are observed. The ground state of Fe^{2+} ions is ^5D . Crystalline field (CF) of cubic symmetry splits the ground state into two multiplets. Since the local symmetry of octahedral positions is of a trigonal type, corresponding distortions

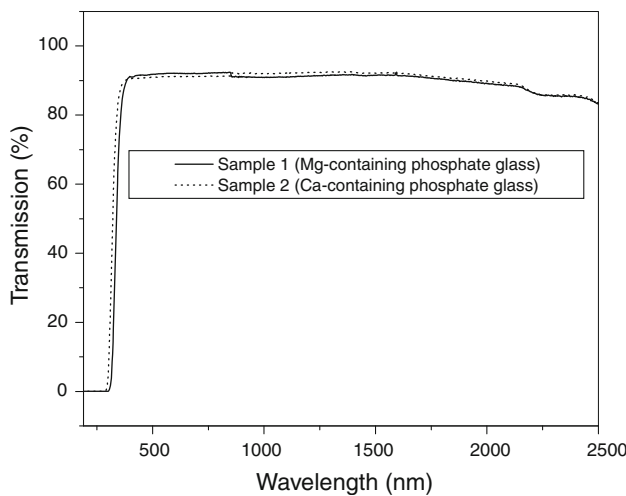


Fig. 1 UV-Vis-NIR transmission spectra of C1 and C2 glass samples

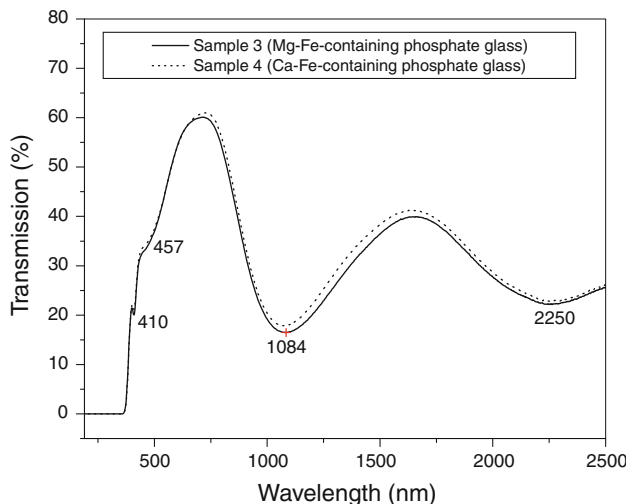


Fig. 2 UV-Vis-NIR transmission spectra of C3 and C4 glass samples

applied to a cubic CF will be distortions of a trigonal type. The ground state 5D of ions Fe^{2+} is split by a cubic field on a doublet 5E_g and triplet $^5T_{2g}$. Trigonal distortions of a cubic field give rise to split of a triplet $^5T_{2g}$ on a doublet $^5E_{g1}$ and singlet A_g [14].

The absorption band placed at about 1084 nm corresponds to the transition $^5T_{2g} \rightarrow ^5E_g$ and the one placed at about 457 nm corresponds to the transition $^6A_1(e^2t_2^3) \rightarrow ^4A_1(e^3t_2^2)$ [15]. However, it is well known that the iron ions enter the glass network both as vitreous matrix modifier and former, providing a mixed structure containing P–O–Fe bonds together with P–O–P bonds [16]. Therefore, not only the optical properties but also the structural properties of the glasses are expected to be influenced by the iron addition.

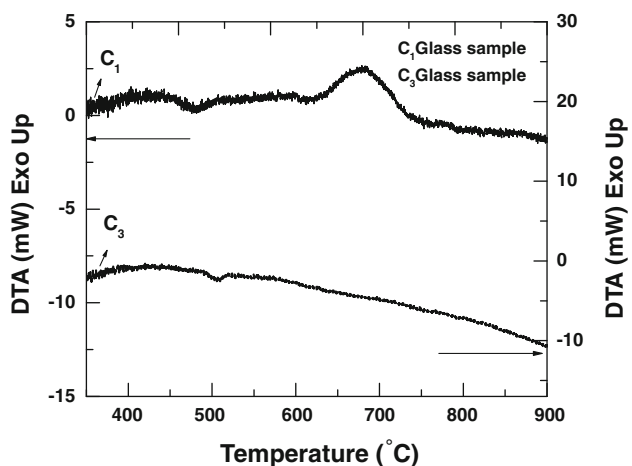


Fig. 3 DTA graphs of C1 and C3 glass samples, in the range 300–1000 °C

Structural changes of the glass network have been studied by DTA measurements [17, 18]. DTA thermal effects for the sample C1 (Fig. 3) reveals an endothermic peak at 480 °C characteristic for the vitreous transition temperature, T_g and an exothermic one at 682 °C attributed to a crystallization process that occurs during the heat treatment. This is in agreement with XRD analysis (Fig. 5a) which put in evidence the formation of crystalline ortho and metaphosphates. When iron is added in the glass composition (C3 glass sample), T_g is slightly increasing at 507 °C as compared with C1 sample and the thermal effects like crystallization could be noticed in DTA graph.

The thermal effects for the sample C2 (Fig. 4) are placed at 504 °C, characteristic for T_g and at 675 °C, where the endothermic peak suggest only a local rearrangement of the glass network. No other thermal effects like crystallization could be noticed in the DTA graph.

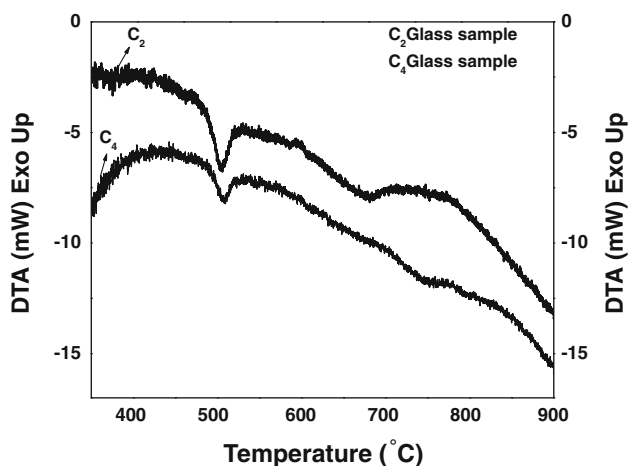
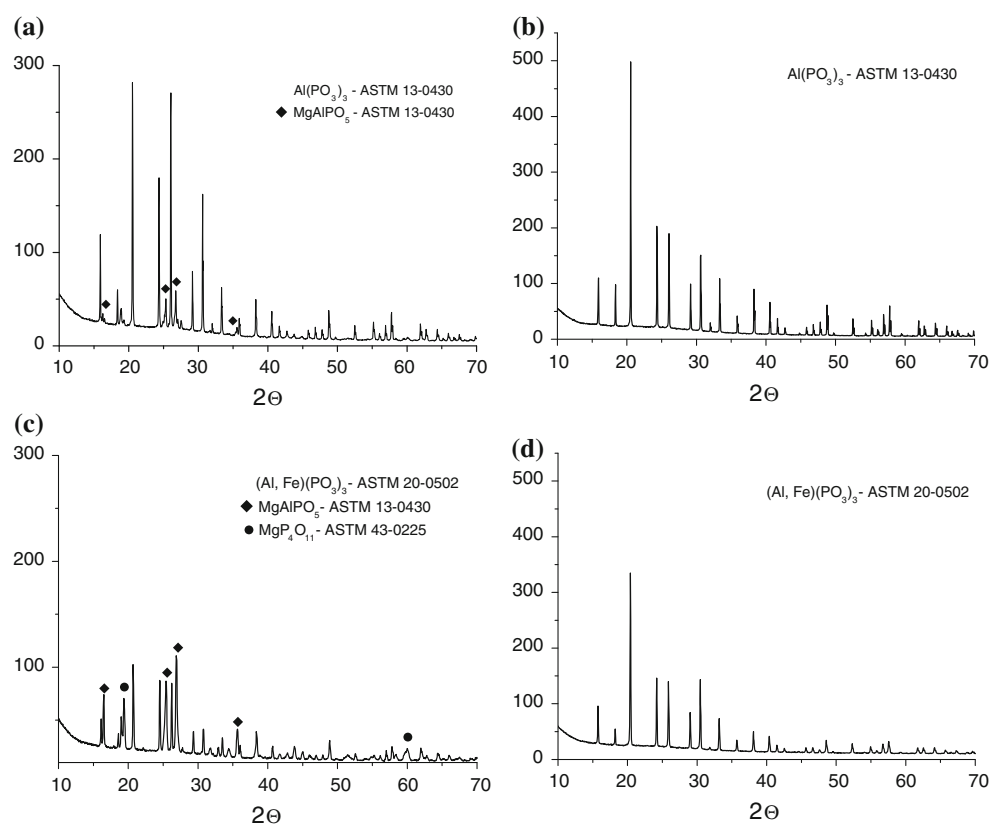


Fig. 4 DTA graphs of C2 and C4 glass samples, in the range 300–1000 °C

Fig. 5 X-Ray diffraction pattern of glass samples: **a** C1; **b** C2; **c** C3, and **d** C4, heat treated at 700 °C



Finally, DTA graph of C4 glass sample (see Fig. 4) shows an endothermic effect at 507 °C, corresponding to T_g and a very weak one at 739 °C, again possibly assigned to local rearrangements of the vitreous structure. So, we are able to claim that the substitution of MgO by CaO causes an increasing of T_g (by 27° C) in samples without Fe, but almost no modification of T_g in Fe-containing samples [9].

Interesting information about the crystalline phases issued within the glass network, after heat treatment at about 700 °C, for 2 h, is presented in the Fig. 5. The values of T_g revealed by DTA graphs are close to T_g values determined by thermal expansion analysis, especially for C3 and C4 samples [9].

As it can be seen from Fig. 5a, XRD pattern for C1 glass samples reveals the presence of two crystalline phases, magnesium aluminum orthophosphate and aluminum metaphosphate. In the case of C3 sample (Fig. 5c), besides two crystalline phases, magnesium pyrophosphate and magnesium aluminum orthophosphate, the addition of iron oxide in the glass composition brings about a crystalline phase formation, iron aluminum metaphosphate. The glass with calcium oxide, without iron oxide, that is C2 sample (Fig. 5b) reveals the presence of the same aluminum metaphosphate as in the case of C1 sample. The addition of iron oxide (Fig. 5d) leads to the formation of the same iron aluminum metaphosphate as in the case of C3 sample.

In the Fig. 5a–d, in order to avoid the overfilling of the diffraction patterns, the peaks without marking signs are assigned to the compound from the legend, free of any marking sign. XPS analysis made on these glasses and reported in [9] confirmed the partial oxidation of Fe^{2+} ions from the starting reagent into Fe^{3+} ions that enter metaphosphate crystalline network. It is well known that the vitreous phosphate network determines the change of the oxidation states of polyvalent transition ions towards higher values. The graphs b and d from Fig. 5 show that no crystalline phases containing calcium ions could be detected in the samples C2 and C4.

The oxidation states and coordination symmetry of iron from C3 and C4 samples have been investigated by EPR spectroscopy. EPR absorption spectra of C3 and C4 samples recorded at room temperature are shown in Figs. 6 and 7, respectively. The C1 and C2 samples did not reveal any EPR signal, proving that the only EPR active paramagnetic species in the glasses are the iron ions.

It is well known that iron ions exist in the glass network in different valence states, with different local symmetries, e.g., Fe^{3+} ions with tetrahedral and octahedral symmetry and Fe^{2+} ions with octahedral symmetry [19]. The amount of iron of different valence states and local coordination depends on the nature and the concentration of the modifier and forming compounds in the glass matrix and on the

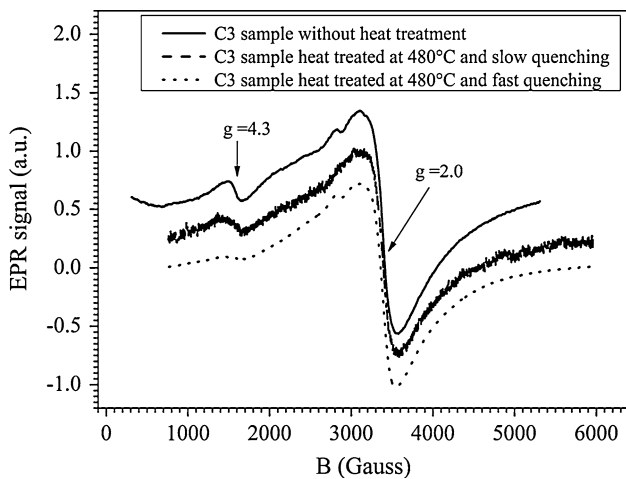


Fig. 6 EPR spectra of C3 glass sample, without annealing (*solid lines*) and after annealing at 480 °C and subsequent slow quenching (*dashed lines*) (SQ) and fast quenching (*dotted lines*) (FQ)

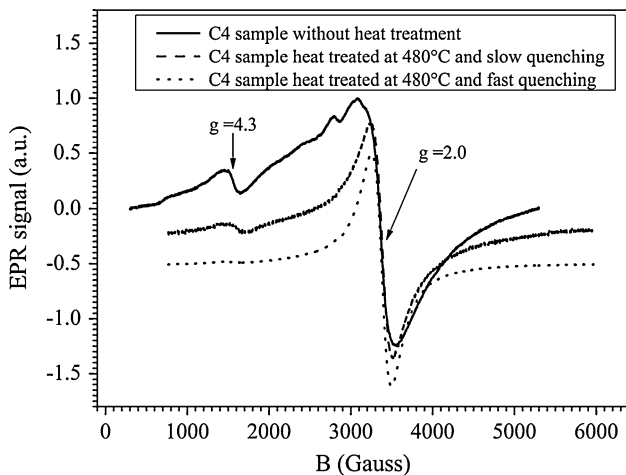


Fig. 7 EPR spectra of C4 glass sample, without annealing and after annealing (*solid lines*) at 480 °C and subsequent slow quenching (SQ) (*dashed lines*) and fast quenching (FQ) (*dotted lines*)

strength of the crystal field. Moreover, when the concentration of the paramagnetic species is higher than a few ppm, an addition dipole–dipole and/or superexchange interaction is observed in EPR spectra.

Both Fe^{2+} and Fe^{3+} may enter as paramagnetic ions in the glass matrix, but only Fe^{3+} ions ($3d^5$, ${}^6\text{S}_{5/2}$) give paramagnetic resonance signal (EPR absorption) at room temperature [20]. Therefore, EPR spectra shows the absorption lines of Fe^{3+} ions involved in structural units with different symmetries. The line characteristics (intensity and linewidth) depend on the nature of the interactions that occur between the paramagnetic species.

As one can see from Figs. 6 and 7, the main lines of EPR spectra of samples C3 and C4 are characterized by

$g = 4.3$ and 2.0, respectively. The above mentioned values for g are directly obtained from the resonance fields of about 3350 and 1551 G, respectively. The EPR absorption line from $g = 4.3$ (corresponding to the low magnetic field at about 1551 G) is due to Fe^{3+} ions which are isolated in the glass network and situated in sites of distorted octahedral symmetry (i.e., rhombic coordination symmetry) subjected to strong crystal field effects [21–24]. On the other hand, due to relative high iron concentration (see Table 1), the iron atoms tend to form clusters (microaggregates) characterized by superexchange and/or dipole–dipole interactions. Therefore the $g = 2$ line (from high magnetic field at about 3350 G) may be attributed to the presence of Fe^{3+} ions forming clusters in octahedral sites, with low crystal field [6].

Further on we present an investigation of the iron distribution and hence, of the clusters in the glass network, revealed by the modifications of the intensity and shape of EPR signal. Thus, C3 and C4 samples were annealed at 480 °C (below the vitreous transition temperature), for 2 h and then they were quenched in two regimes: slow (SQ) and fast (FQ). In SQ regime the samples were quenched in the furnace atmosphere and in FQ regime they were quenched outside the furnace, put in closed vials and immersed in cold water.

As we see from Figs. 6 and 7, the EPR signal at $g = 2$ is influenced by the applied heat treatment. In the case of C3 sample it is to be noticed a smooth change of the peak to peak linewidth from 413(5) G to 456(5) G (SQ) and 415(5) G (FQ). For C4 sample, the line at $g = 2$ show a stronger change of the peak to peak linewidth from 424(5) G to 270(5) G (SQ) and 242(5) G (FQ). At relative high iron oxide amount as in the case of our samples (higher than 4 mol%), the width of the line at $g = 2.0$ is determined by super-exchange and dipole–dipole interactions between iron ions within the micro-aggregates, providing $\text{Fe}^{3+}\text{--Fe}^{3+}$ or $\text{Fe}^{3+}\text{--Fe}^{2+}$ pairs. In the case of C3 sample, there is a small change of the iron clusters distribution induced by annealing, as suggested by the smooth variation of the line width. In the case of C4 sample, the influence of the annealing process on the line width at $g = 2.0$ is much more important than in case of C3 sample, suggesting an increasing of the iron agglomeration induced by the thermal treatment and subsequent quenching (Fig. 7). Inside the clusters, due to the interactions between iron ions, the surrounding oxygen field intensity (the crystal field) is diminished and we deal with much less distorted rhombic coordination symmetry. As it can be seen from Fig. 7, the FQ line becomes symmetrical with a lorentzian line shape. At the same time, a diminution of the EPR signal at $g = 4.3$ is induced by thermal annealing. The signal almost disappears after FQ.

This is an additional proof that an ordered phase of iron ions appears in the glass network on the expense of the much disordered configurations of isolated Fe^{3+} of low symmetry, the super-exchange interactions between the formed species being dominant [25]. The decreasing signal at $g = 4.3$ (sign of an increased clusterization) is faster in samples with Ca ions compared with samples based on Mg ions and also is faster for the FQ regime, compared with the SQ regime.

Additional information on the oxidation states and coordination symmetry of iron in C3 and C4 samples without additional heat treatment has been obtained by Mossbauer spectroscopy. The ^{57}Fe Mossbauer spectra of the two samples, collected at room temperature (RT) are shown in Fig. 8.

Both spectra put in evidence the presence of two types of paramagnetic iron ions [26, 27]. The best fit was obtained by using two paramagnetic doublets for each spectrum. The corresponding fitted Mossbauer parameters (isomer shift, IS, quadrupole splitting, QS, and the relative population of each iron site, obtained via the relative area of the spectral Mossbauer component, R.A.) are presented in Table 2. The oxidation state and oxygen coordination around the central iron, as suggested by the values of the hyperfine parameters, are shown in the same table.

The first paramagnetic component which appears in each spectrum is a central doublet with an isomer shift of about 0.40 mm/s, typical to Fe^{3+} ions with sixfold oxygen

coordination. The quite large value of the quadrupole split (around 0.70 mm), connected only to the lattice contribution in case of the Fe^{3+} ion with its symmetrical electron distribution, infers a relatively high distorted configuration around the central ion, in agreement with EPR data. However, in order to make a distinction between isolated Fe^{3+} ions and aggregated Fe^{3+} ions (forming most probable nanosized oxide particles), additional Mossbauer spectra at very low temperatures will be presented further. On the other side, the advantage of the Mossbauer spectroscopy over EPR is related to the possibility to see iron in oxidation states different of 3+. Consequently, the second paramagnetic component of the room temperature Mossbauer spectra is a doublet with an isomer shift of more than 1.2 mm/s, typical to Fe^{2+} ions also with sixfold oxygen coordination. This time, the high quadrupole splitting (more than 2.30 mm/s) is mainly due to the contribution of the sixth electron. The only notable difference between spectra belonging to C3 and C4 samples, respectively, is the different relative amount of the Fe^{2+} ions, which is clearly increasing in the sample prepared with CaO (C4) as compared with the sample prepared with MgO (C3).

The Mossbauer spectra collected on samples C3 and C4 at 4.5 K are shown in Fig. 9 in order to observe the iron clustering process. As it is well known, small clusters of Fe (or Fe oxides) can behave above the blocking temperature as superparamagnetic phases giving rise in the Mossbauer spectrum to the usual central patterns (singlet or doublets). As soon as the measurement temperature is going below the blocking temperature, the clusters show net effective magnetic moment giving rise in the Mossbauer spectrum to the usual magnetic sextet specific to Fe configurations with magnetic order. Therefore, the significant advantage of the Mossbauer spectra collected at low temperature is related to the fact that they show on one hand the relative amount of Fe which is clustering and on the other hand, provide direct information about the clustering phase. As can be observed, both spectra collected at 4.5 K show the presence of a magnetic sextet, proving the presence of the Fe clusters, in agreement with the EPR data. The Mossbauer parameters corresponding to the spectral components, as well as their relative area are shown in Table 3.

The magnetic pattern consists of a broad sextet with an isomer shift of 0.52 mm/s and a hyperfine field of about 53.5 T, which are both typical to Fe^{3+} ions. In addition, the value of the average hyperfine field restricts the type of Fe phases in the cluster to only hematite and magnetite. Corroborating the above results with the large linewidth (more than 2 mm/s), one may conclude we deal with a large size distribution of very fine clusters consisting most probably of a mixture of hematite and magnetite, where the intra-cluster magnetic order is induced by super-exchange interactions. Only about 23% of the total Fe in the sample

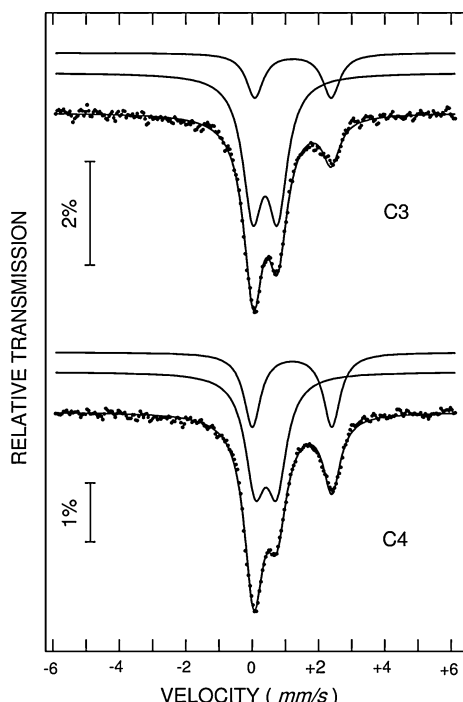


Fig. 8 Room temperature ^{57}Fe Mossbauer spectra of C3 and C4 glass samples

Table 2 Room temperature Mossbauer components of the analyzed samples and corresponding spectral parameters

Samples	Mossbauer components	IS (mm/s)	QS (mm/s)	R. A. (%)	Oxidation states	Oxygen coordination
C3	Doublet 1	0.40 (1)	0.75 (1)	77 (1)	Fe ³⁺	6
	Doublet 2	1.24 (1)	2.30 (2)	23 (1)	Fe ²⁺	6
C4	Doublet 1	0.42 (1)	0.65 (1)	62 (1)	Fe ³⁺	6
	Doublet 2	1.21 (2)	2.40 (3)	38 (1)	Fe ²⁺	6

The oxidation state and the coordination of different iron sites are also presented

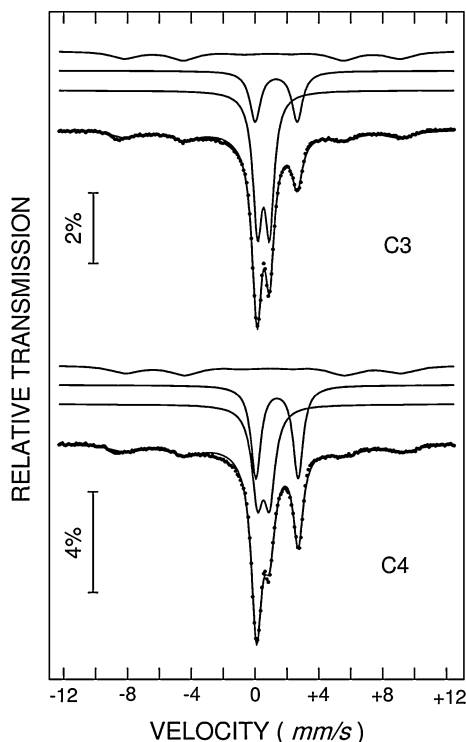


Fig. 9 ^{57}Fe Mossbauer spectra of C3 and C4 glass samples, collected at 4.5 K

is embedded in the clusters, the rest of about 77% being present as isolated ions with octahedral oxygen coordination. The isolated ions could be either Fe^{3+} or Fe^{2+} , their relative amount being in a ratio close to 2:1 in the sample

prepared with MgO (C3) and close to 1:1 in the sample prepared with CaO (C4).

Conclusions

The investigation of iron-doped phosphate glasses was aimed at obtaining information on the redox state and coordination symmetry of iron ions in the glass network. UV-vis-NIR spectra revealed that both Fe^{2+} and Fe^{3+} ions are present in the vitreous matrix, possibly as network modifier as well as network former. TG graphs showed a very low weight change during the heat treatment in the range 300–1000 °C. All DTA curves presented an endothermic effect ranged between 480 and 507 °C, corresponding to the vitreous transition temperature, with higher values for iron-containing samples. In the case of magnesium oxide-containing sample, without iron, DTA curve showed an exothermal effect corresponding to a crystalline phase formation whereas calcium oxide-containing samples exhibit a low endothermic effect, probably due to local rearrangements of the glass network. Phosphate crystalline phases formed in the glass structure, after the heat treatment at about 700 °C are revealed by XRD analysis. EPR spectra put in evidence signals proving the existence of Fe^{3+} paramagnetic ions with rhombic symmetry of bonded oxygen atoms. Centers belonging to isolated Fe^{3+} as well as to Fe^{3+} ions forming clusters are evidenced. The annealing of the glass samples containing iron ions, at temperature below the vitreous transition temperature, influences the iron distorted octahedral configuration, in a

Table 3 Mossbauer components of the analyzed samples at 4.5 K and corresponding spectral parameters

Samples	Mossbauer components	IS (mm/s)	QS (mm/s)	B _{hf} (T)	R. A. (%)	Oxidation states	Clustering degree
C3	Doublet 1	0.53 (1)	0.76 (1)	–	54 (1)	Fe ³⁺	Isolated
	Doublet 2	1.32 (1)	2.64 (2)	–	24 (1)	Fe ²⁺	Isolated
	Sextet	0.47 (1)	−0.09 (2)	53.6 (1)	22 (1)	Fe ³⁺	Cluster-like
C4	Doublet 1	0.52 (1)	0.65 (1)	–	40 (1)	Fe ³⁺	Isolated
	Doublet 2	1.37 (2)	2.65 (3)	–	37 (1)	Fe ²⁺	Isolated
	Sextet	0.52 (1)	−0.12 (2)	53.5 (1)	23 (1)	Fe ³⁺	Cluster-like

The oxidation state and the clustering degree are also presented

greater extent in the case of CaO containing glass in comparison with MgO containing sample. Mossbauer spectra at room temperature, in the case of C3 and C4 glass samples shows both Fe²⁺ and Fe³⁺ paramagnetic ions in distorted octahedral configuration, the oxidized species being dominant. Moreover, low temperature Mossbauer spectra evidence the clustering process of about 23% from the total iron, the rest of 77% forming isolated Fe ions. The relative amount of Fe²⁺ and Fe³⁺ isolated ions is different in the two samples, prepared with MgO and CaO, respectively. These results are qualitatively in agreement with both EPR and UV-vis-NIR data, but quantitatively, the observed difference in the relative amount of isolated Fe²⁺ and Fe³⁺ species is not reflected in the UV-vis-NIR spectra.

Acknowledgements The authors are grateful to the Romanian Executive Agency for Higher Education and Research Funding, for the financial support in the frame of RP-8/2007 project-PN II Human Resources and PN 09-27.02.02/27.02.2009 (Nucleus Programme 2009–2011). The authors of the article are also grateful to Dr. Marin Cernea from the National Institute of Physics of Materials, Magurele, Romania for XRD measurements and invaluable discussions and suggestions on the crystalline phase formation within phosphate glass network.

References

- Murawski L (1982) J Mater Sci 17:2155. doi:[10.1007/BF00543723](https://doi.org/10.1007/BF00543723)
- Kumar B, Chen C, Lin S (1992) Phys Chem Glass 33:204
- Sanad AM, Kashif I, Khaled MA, Aly SA, Farouk H (1988) Phys Chem Glass 30:27
- Stefanovskii SV, Ivanov IA (1994) Glass Phys Chem 20(2):103
- Brow RK, Arens CM (1994) Phys Chem Glass 35(3):132
- Albon C, Muresan D, Vandenberghe RE, Simon S (2008) J Non-Cryst Solids 354:4603
- Sales BC, Boatner LA (1986) J Non-Cryst Solids 79:83
- Sava BA, Diaconu A, Ursu LD, Boroica L, Elisa M, Grigorescu C, Vasiliu C, Stamatin I, Nastase F, Nastase C, Dumitru A (2008) Adv Mat Res 39–40:667
- Elisa M, Sava BA, Diaconu A, Boroica L, Ursu D, Stamatin I, Nastase F, Nastase C (2009) Glass Phys Chem 35(6):596
- Elisa M, Vasiliu C, Meghea A, Iftimie N, Giurginca M, Trodahl HJ, Dalley M (2005) Phys Chem Glass 46(6):499
- Elisa M, Vasiliu IC, Grigorescu CEA, Grigoras B, Nicu H, Nicu D, Meghea A, Iftimie N, Giurginca M, Trodahl HJ, Dalley M (2006) J Opt Mat 28(6–7):621
- Elisa M, Grigorescu CEA, Vasiliu IC, Bulinski C, Kuncser V, Predoi D, Filoti G, Meghea A, Iftimie N, Giurginca M (2005) Rev Adv Mat Sci 10:34
- Elisa M, Vasiliu C, Grigorescu C, Striber J, Radu D, Trodahl JH, Dalley M (2006) J Opt Adv Mat 8(2):810
- Gareyeva ZV, Doroshenko RA (2004) J Magn Magn Mater 268:1
- Bergo P, Pontuschka WM, Prison JM (2008) Mater Chem Phys 108:142
- Muresan D, Bathorya D, Keula M, Balasz I, Simon S (2005) J Opt Adv Mat 7(6):2835
- Flynn JH (1974) Therm Acta 8:69
- Dollimore D (1992) Therm Acta 203:7
- Chakradhar RPS, Murali A, Rao JL (1998) Opt Mat 10:109
- Rao AS, Reddy RR, Rao TVR, Rao JL (1995) Solid State Com 96:701
- Kliava J, Berger R, Servant Y, Emery J, Gren JM, Troc J (1996) J Non Cryst Solids 202:205
- Rajendra KS, Kothiyal GP, Srinivasan A (2008) J Non Cryst Solids 354:3166
- Cozar O, Magdasa A, Vedeanu BN, Ardelean I (2008) J Opt Adv Mat 10(12):3202
- Reiss ST, Faria DA, Martinelli JR, Pontuschka WM, Day DE, Partiti CSM (2002) J Non Cryst Solids 304:188
- Ardelean I, Peteanu M, Filip DS, Simon V, Gyirffy G (1997) St Comm 102(4):341
- Greenwood NN, Gibb TG (1971) Mossbauer spectroscopy. Chapman and Hall Ltd, London
- Russo U, Carbonin S, Della Giusta A (1995) Iron distribution among various valence states and coordination geometries in natural spinels. Proceedings of XXX Zakopane School of Physics, Zakopane p 254